Simultaneous measurement of aqueous redox-sensitive elements and their species across the soil-water interface

YUAN, ZF, GUSTAVE, W, SEKAR, R, BRIDGE, Jonathan <http://orcid.org/0000-0003-3717-519X>, WANG, JY, FENG, WJ, GUO, B and CHEN, Z

Published version

YUAN, ZF, GUSTAVE, W, SEKAR, R, BRIDGE, Jonathan, WANG, JY, FENG, WJ, GUO, B and CHEN, Z (2021). Simultaneous measurement of aqueous redox-sensitive elements and their species across the soil-water interface. Journal of Environmental Sciences (China), 102, 1-10.

Simultaneous measurement of aqueous redox-sensitive elements and their species across the soil-water interface

Zhao-Feng Yuan [1, 2, 3], Williamson Gustave [1, 2, 4], Raju Sekar [5], Jonathan Bridge [6], Jia-Yue Wang [1], Wei-Jia Feng [1], Bin Guo [7 *] and Zheng Chen [1 *]

[1] Department of Health and Environmental Sciences, Xi'an Jiaotong-Liverpool University, 111 Ren'ai Road, Suzhou, Jiangsu 215123, China. E-mail: ebiogeochem@outlook.com

[2] Department of Environmental Science, University of Liverpool, Brownlow Hill, Liverpool L69 7ZX, UK.

[3] Department of Plant Science, Tarim University, Alaer, Xinjiang 843300, China.

[4] Chemistry, Environmental & Life Sciences, University of The Bahamas, New Providence, Nassau, The Bahamas.

[5] Department of Biological Sciences, Xi'an Jiaotong-Liverpool University, 111 Ren'ai Road, Suzhou, Jiangsu 215123, China.

[6] Department of Natural and Built Environment, Sheffield Hallam University, Howard St, Sheffield S1 1WB, UK.

[7] Institute of Environment, Resource, Soil and Fertilizer, Zhejiang Academy of Agricultural Sciences, Hangzhou, 310021, China.

Received 31 July 2020

Revised 31 August 2020

22

Abstract: The redox-sensitive elements, such as iron, manganese, sulfur, phosphorus, and arsenic, shift their speciation every millimeter (mm) across the soil-water interface in the flooded soil environments. Monitoring of element speciation at this high-resolution (HR) within the SWI is still difficult. The key challenge lies in obtaining sufficient porewater samples at specific locations along the soil gradient for downstream analysis. Here with an optimized inductively coupled plasma mass spectrometry (ICP-MS) method and a HR porewater sampler, we demonstrate mm-scale element profiles mapping across the SWI in paddy soils. High-concentrations of iron and manganese (> 10 $mg \cdot L^{-1}$) were measured by ICP-MS in an extended dynamic range mode to avoid signal overflow. The iron profile along the SWI generated by the ICP-MS method showed no significant difference ($p < 0.05$) compared to that measured independently using a colorimetric method. Furthermore, four arsenic (arsenite, arsenate, monomethylarsonic and dimethylarsinic acid), two phosphorus (phosphite and phosphate) and two sulfur (sulfide and sulfate) species were separated in 10 min by ion chromatography -ICP-MS with the NH_4HCO_3 mobile phase. We verified the technique using paddy soils collected from the field, and present the mm-scale profiles of iron, manganese, and arsenic, phosphorus, sulfur species (relative standard deviation < 8%). The technique developed in this study will significantly promote the measurement throughput in limited samples (e.g. 100 μL) collected by HR samplers, which would greatly facilitate redox-sensitive elements biogeochemical cycling in saturated soils.

44

Keywords:

porewater

soil-water interface

arsenic

iron

manganese

sulfur

species

---

* **Corresponding author.** E-mail: ebiogeochem@outlook.com (Zheng Chen); Email: ndgb@163.com (Bin Guo)

1. Introduction

In flooded soils, the chemical environments of the surface water and saturated sediment porewater are very different. The surface water is oxidizing due to the high dissolved O_2, however, the sediments are generally reducing owing to the lack of O_2 and the abundance of organic matter (Frenzel et al., 1992). The O_2 can only penetrate the upper sediment to a depth of a few millimeters (mm) (Ratering and Schnell, 2001). As a result, the narrow boundary zone between the surface water and sediments, i.e. soil-water interface (SWI), displays a sharp redox decrease with depth (Huo et al., 2015; Jones et al., 2018). Iron (Fe), manganese (Mn), and sulfur (S) are the most important elements in SWI, existing in both solid and dissolved phases through complex redox reactions (Peng et al., 2019). The redox processes of Fe, Mn, and S significantly impact the fate of many elements of environmental and agricultural concern, such as arsenic (As) and phosphorus (P) (Gao et al., 2016; Gao et al., 2006; Mcadams et al., 2016; Pi et al., 2018). Although it is of great importance to study the behavior of these elements in SWI, the high-resolution (HR) mm-scale mapping of those elements and their species has been severely limited to date by the lack of suitable available methods.

Many efforts have been made to measure the mm-scale element profile in porewater along SWI. The diffusive gradient in thin films technique (DGT) is one of the best, which can even depict the elements' pattern in μm scale, however it measure the flux instead of the equilibrated concentration (Davison and Zhang, 1994; Fang et al., 2018; Yin et al., 2020). The equlibrated concentrations can be measured by the diffusive equilibrium in thin films (DET) technique and *in situ* equilibrium dialysis samplers (peeper) (Arsic et al., 2018; Bottrell et al., 2007; Di et al., 2012; Dočekalová et al., 2002; Guan et al., 2015; Monbet et al., 2008). The DET probe resolution is 2 mm when using the strip-cutting method (Dočekalová et al., 2002; Gao et al., 2007), and can reach 1 mm when combining reagent dying and computer imaging densitometry detection (Bennett et al., 2012b; Robertson et al., 2008). Peepers have relatively low spatial resolution (~ 5 mm) compared to DET because handling the water in peeper chambers is not as convenient as the gels in DET probe (Di et al., 2012; Wen et al., 2019). Recently, we developed a novel porewater sampler, called *In-situ* Porewater Iterative (IPI) sampler, to monitor the mm-scale heterogeneity of trace metals in saturated soils (Yuan et al., 2019). The IPI sampler has a comparable HR (~ 2 mm) as DET probe. Unlike DET and peeper, the IPI sampler can be used repeatedly at a certain place without need for removal or destructive sampling. Another advantage of IPI samplers is to obtain clean liquid porewater sample directly, which is almost ready for downstream instrumental analysis. Due to these advantages, the IPI sampler was very suited for mm-scale element profile mapping.

Simultaneous measurement of multi-element profiles at HR across SWI presents significant additional challenges. The sharp and sensitive redox gradient along SWI requires that the porewater volume sampled should be as small as possible to minimize the disturbance to the sampling environment (Seeberg‐Elverfeldt et al., 2005), and yet large enough to meet the minimum sample size for sensitivity and specificity analysis of all the interested parameters (Arsic et al., 2018; Bennett et al., 2012a; Ding et al., 2016; Motelica-Heino et al., 2003). The HR samplers (e.g. DET, HR peeper, IPI samplers) designed for element profile mapping generally can only take less than 0.5 mL solution (Yuan et al., 2019), which is a bare minimum for one sample injection with most analytical techniques, like inductively coupled plasma mass spectrometry (ICP-MS) (Xu et al., 2017), ICP- optical emission spectrometry (Cheng et al., 2012), colorimetric method (Lumbaque et al., 2019). An alternative to collect more samples is to collect porewater repeatedly at different places or times, assuming the soil or sediment matrix is homogenous and stable over time. However, this assumption is severely limiting and constrains the ability to probe the heterogeneity and dynamics of SWI biogeochemistry as a function of location and in response to changing environmental conditions (Arsic et al., 2018; Yuan et al., 2019). Thus, it would be better to solve the issue by optimizing the analytical techniques used in extracting data from the samples.

ICP-MS has been widely applied to understand the element behaviors in various environments due to its broad spectrum and very low detection limits (Cotta and

117 Enzweiler, 2009). Studies of rhizospheric element profiles have greatly benefited
118 from developments in ICP-MS technologies. For example, the combination of laser
119 ablation (LA)-ICP-MS with DGT allows mapping of μm-scale element fluxes and
120 provided key information for understanding As behaviors on the root apexes
121 (Williams et al., 2014). More recently, a new approach, called extended dynamic
122 range (EDR), was introduced to simultaneously measure major and trace metals by
123 ICP-MS (Hilbig et al., 2017). The EDR mode can attenuate the counts of selected
124 elements through the spectrometer by tuning the 'rejection parameter a' (Rpa), thus it
125 enables the detection of major and minor elements in a single run (Hilbig et al., 2017).
126 EDR mode is potentially ideal to measure multi-element concentrations in
127 volume-limited samples, such as the porewater sampled by HR samplers, which
128 contains Fe and Mn over 10 $mg \cdot L^{-1}$, and other traces at $\mu g \cdot L^{-1}$ concentrations.
129 However, the combination of HR samplers and ICP-MS under EDR mode has not
130 been tested to date.

131 The small porewater sample volume also hinders the measurement of element
132 speciation. Arsenic, P and S species play crucial roles in aquatic biogeochemical
133 cycling (Chen et al., 2019; Sun et al., 2017). Traditionally, phosphate, P(V), is
134 measured by colorimetry (molybdate blue) (Rietra et al., 2001), sulfide, S(-II), by
135 micro-electrode and spectrophotometric method (Laskov et al., 2007), sulfate, S(VI),
136 by ion chromatography (IC) (Keller-Lehmann et al., 2006), arsenite and arsenate,
137 As(III,V), by IC-ICP-MS (Gallagher et al., 2001). Summing up, to measure all these

138 analytes in a single sample by standard methodologies, it requires an aliquot volume
139 of several mL, far more than the porewater volume collected from HR samplers (Xu
140 et al., 2012; Yuan et al., 2019). Among methods noted here, IC-ICP-MS can measure
141 all the species, but is limited to the appropriate mobile phase. A review of the
142 literature (Chen et al., 2019; McDowell et al., 2004; Morton et al., 2005; Reid et al.,
143 2020; Suzuki et al., 2009) revealed that NH_4HCO_3 mobile phase, which is free of As,
144 P, and S, can separate P, S and As species. Combined with the ICP-MS method
145 (Hilbig et al., 2017), use of NH_4HCO_3 elution IC-ICP-MS thus presents the possibility
146 of accurate and rapid quantification of key major and minor element concentration
147 and speciation within SWI profiles from small samples obtained by HR samplers such
148 as IPI (Yuan et al., 2019), enabling non-destructive, mm-scale and repeated probing of
149 SWI chemistry over time and therefore overcoming several key limitations of existing
150 approaches outlined above.

151 This study demonstrates simultaneous measurement of multi-element and
152 multi-species concentration profiles in flooded soil porewater using a HR sampler (IPI,
153 after Yuan et al. (2019)) combined with the optimized ICP-MS and IC-ICP-MS
154 method. The typical redox-active elements found in soil porewater, including Fe, Mn,
155 As, P and S, and the common species of As, P, and S, including phosphite (P(III)),
156 P(V), S(-II), S(VI), monomethylarsonic acid (MMA), dimethylarsinic acid (DMA),
157 As(III), As(V), were investigated in flooded paddy soils. This study directly addresses
158 the challenge of maximizing the chemical information obtainable from increasingly

small sample volumes, which would greatly enhance the measurement range, throughput and application potential of HR samplers.

2. Materials and methods

2.1 Reagents and materials

All reagents used in this study were of analytical grade or higher, and purchased from Aladdin Chemical Reagent Co., Ltd. (Shanghai, China), unless stated otherwise. Element standards for calibration, including As, Fe, Mn, P, S as well as P, S, and As species, were supplied by Guobiao (Beijing) Testing & Certification Co., Ltd (Beijing, China). All solutions were prepared with ultrapure water (18.2 MΩ cm, Millipore Corp., Bedford, USA) deoxygenated by bubbling pure N_2 overnight.

Before the soil was sampled from paddy fields in Shaoguan (SG, 25°6'N, 113°38'E), obvious stones and plant debris were mechanically removed by shovels. In total, ~ 50 kg soils from the top layer (0 - 20 cm) were collected. The soils were directly transported to the laboratory, and homogenized by passing through a 1.0 mm diameter wet sieve. The soil characteristics are shown in **Table S1**.

2.2 Porewater sampler preparation

The IPI sampler used in this study has a similar design as described in detail in our

178 previous study (Yuan et al., 2019), with some minor modifications noted here. A novel
179 hollow fiber membrane tube (modified polyethersulfone, 20 nm pore size, inner ×
180 outer diameter × length = 1.0 mm × 1.7 mm × 35 mm, 27.5 μL, Motimo Membrane
181 Technology Co., Ltd., Tianjin, China) and two pipes (PTFE, inner × outer diameter ×
182 length = 0.5 mm × 1.0 mm × 180 mm, 35 μL) were used to construct the IPI sampler.
183 The pore size of the membrane was demonstrated (**Fig. S1**) with scanning electron
184 microscopy (SEM) JSM-7600 (FJEOL Ltd., Japan). The updated membrane does not
185 contain fluoride or other potential chelators, which can avoid the complexation of the
186 membrane for certain analytes (e.g. lead) (Yuan et al., 2019).

187 When the IPI sampler is deployed into solution or saturated soils, solutes around
188 the hollow fiber membrane tube can diffuse through the membrane (**Fig. S2A**). The
189 solution inside the tube is pumped out and collected when the diffusion reaches
190 equilibrium (**Fig. S2B**). During the deployment, silicon caps are applied to seal the IPI
191 sampler to avoid potential contamination (e.g. gasoline) from the atmosphere. During
192 each sampling event, 27.5 μL liquid sample in the sampling tube is mixed with 70 μL
193 ultrapure water in pipes when they are pumped out from the sampler. This indicates ~
194 100 μL porewater sample can be sampled each time by the IPI sampler, with a
195 dilution factor of 3.5.

196 Thirty-four IPI samplers were horizontally assembled side by side in a 3D
197 printed holder (cavity cuboid, length × width × height = 40 mm × 30 mm × 120 mm,
198 **Fig. S2C-E**). The IPI sampler array, i.e. SWI profiler, can sample the porewater every

199 1.7 mm along SWI (**Fig. S2C**). The SWI profiler has a sampling depth of 60 mm and
200 was stored in O_2-free ultrapure water before deploying into flooded soils (**Fig. S2F**),
201 following the procedure described in Yuan et al. (2019).

202

203 **2.3 Analytical method and quality control**

204 Element concentrations were quantified by ICP-MS (NexION 350X, PerkinElmer,
205 Inc., Shelton, CT USA). The conditions were as follows: EDR mode; dynamic
206 reaction cell (DRC) mode (O_2, gas flow, 1.0 mL·min^{-1}); data only analysis; RF power
207 1,600W; plasma gas flow rate 15 L·min^{-1}; auxiliary gas flow 1.2 L·min^{-1}; nebulized
208 gas flow 0.94 L·min^{-1}; nickel sampling and skimmer cones. The Rpa in EDR mode is
209 a voltage parameter, which can tune bandpass of m/z that has stable trajectories
210 (Tanner and Baranov, 1999). This parameter functions for the precursors of target
211 analyte generated from dynamic reaction/collision cell. When Rpa = 0 (default value),
212 a wide range bandpass of *m/z* is obtained, while non-zero Rpa (0 - 0.24) creates a
213 narrow bandpass of *m/z*. The sensitivity of *m/z* is proportional to the width of
214 bandpass, hence the upregulation of Rpa provides an option to suppress the high
215 sensitivity of *m/z* caused by high abundance analyte or potential interferences. When
216 using Rpa under different analytical modes, the Rpa value can be manually set for the
217 interested element.

The porewater sample collected by the IPI sampler was introduced into ICP-MS by a PFA-200 Microflow Nebulizer (0.2 mL·min^{-1} uptake rate). Iron, Mn As, P and S were measured by ICP-MS in EDR and DRC mode. Counts of $^{91}AsO^+$, $^{57}Fe^+$, $^{47}PO^+$, $^{48}SO^+$ and $^{55}Mn^+$ were recorded.

Element species were measured by IC-ICP-MS. The IC (Dionex ICS-1100, Thermo Scientific, USA) consisted of a standard 25 μL sample loop and an anion-exchange column (IonPac AS23, 250 mm × 4 mm, Dionex). Mobile phases used for the separation were 20 mmol·L^{-1} NH_4HCO_3 at pH 10 (Suzuki et al., 2009), with a flow rate of 1.0 mL·min^{-1}. The analytical column was connected to a Type C0.5 Glass Nebulizer of the ICP-MS. The standards were prepared in neutral conditions (pH 7; 100 μg·L^{-1} P(III), P(V), As(III), As(V), MMA and DMA; 1 mg·L^{-1} S(-II) and S(VI)).

When developing the calibration curve, a series of standard solutions, containing 1.0/10/100, 2.0/20/200, 5.0/50/500, 10/100/1000, 20/200/2000 μg·L^{-1} As&Mn/P/Fe&S in 2% HNO_3, were measured (n = 3). For As, P and S species, a series of standard solutions, containing 0/0/0, 1.0/20/500, 2.0/50/1000, 5.0/100/2000, 10/200/5000 μg·L^{-1} DMA/P(V)/S(VI) under pH 7, were measured. Peak area was used to fit the standard curve, and three times standard deviation was used to calculate the limit of detection (LOD). Data quality was assured by testing a spiked standard after every 30 samples.

2.4 The sampling of total elements and element species by IPI samplers

Total elements were prepared in acidic conditions (pH 2; 10 μg·L^{-1} As and Mn; 10 mg·L^{-1} Fe, P, and S), and As species were prepared in neutral conditions (pH 7; 100 μg·L^{-1} As(III), As(V), MMA and DMA). Those solutions were made by diluting the relative standards with ultrapure water. To determine the equilibrium time required for IPI samplers to sample Fe, Mn, As, P, S as well as As species, the time-dependent response of the sampler to those solutes was investigated in solutions. The samples inside the samplers were measured after 0, 0.5, 1, 3, 6, and 12 hr equilibrium time by ICP-MS or IC-ICP-MS.

2.5 Multi-element profile mapping

To detect the element profile, the SWI profilers were inserted into flooded soils in a pot (diameter × height = 12 cm × 20 cm), with 10 mm above SWI and 50 mm in soils (**Fig. S2C**). Two replicates were conducted.

The paddy pot soils were filled with ultrapure water with ~ 3 cm overlying water, and the water depth was maintained daily by supplementing ultrapure water during the experiment. The soils were allowed to stabilize (22 °C, dark conditions) for three months before the deployment of SWI profilers. Before sampling, the solution inside IPI samplers was replaced by O_2-free ultrapure water driven by an injection pump (TYD01, Lei Fu, China) (**Fig. S3**), with a velocity of 1.0 mL·min^{-1}.

Based on the equilibrium test of analytes in this study, the sampling interval was set as 24 hr. The sampled solution was preserved in the O_2-free EDTA solution (Gallagher et al., 2001). The EDTA solution (2 $g \cdot L^{-1}$) was online mixed with the porewater in a 1:3 volume ratio driven by two injection pumps (**Fig. S3**), with a velocity of 0.25 and 0.75 $mL \cdot min^{-1}$ respectively. The mixed sample was carefully collected in a clean 0.6 mL centrifuge tube. In total, ~ 100 μL porewater was collected with an EDTA concentration of 500 $mg \cdot L^{-1}$. Each sample was divided into two parts (~ 50 μL per part) and measured by ICP-MS and IC-ICP-MS respectively. Additionally, a microplate reader was used to measure the Fe profile in paddy soil with the 1, 10-phenanthroline method (λ = 510 nm) (Lumbaque et al., 2019). Before measurement, the O_2-free colorimetric reagent was online mixed with the porewater sample in a 1:1 volume ratio driven by two injection pumps (**Fig. S3**), and ~ 200 μL solution was collected and transferred into 96-well plate (200 μL) for absorbance determination in a microplate reader (Tecan-Spark, Tecan Trading AG, Zurich, Switzerland). Finally, mm-scale profiles of multi-element and multi-species were mapped and evaluated.

2.6 Data analysis

R software (version 3.5.0) was used to analyze and plot the data in this study. We used the standard deviation to show the variance of the data. Data of different methods

were subjected to one-way analysis of variance (ANOVA) to determine statistical significance ($p < 0.05$) using SPSS 22 software (SPSS Inc., Chicago, USA).

3. Results and discussion

3.1 The time-dependent sampling efficiencies of Fe, Mn, As, P and S by IPI samplers

Initially, the trans-membrane diffusion of Fe, Mn, As, P, and S in solution condition was studied. This was done to determine the applicability of IPI samplers in collecting solutions with those elements, which is a prerequisite before using the sampler to collect those elements in soil porewater. Significant peaks of all the five elements were observed with a 50 μL solution (**Fig. S4**). The equilibration test showed the concentrations of those elements increased rapidly in the first three hr, and then reached a plateau representing their concentration in solutions (**Fig. S5**). The time-dependent curves were consistent with our previous report for As, antimony, cadmium, lead, and nickel (Yuan et al., 2019). Considering the presence of dissolved organic matters, which could slow down the diffusion of solutes (Dočekalová et al., 2002; Reynolds et al., 2004; Yuan et al., 2019; Zhai et al., 2018), we deployed the IPI sampler at 24 hr equilibration period in saturated soils.

3.2 The effect of Rpa value on Fe and Mn detection

The Fe and Mn signals can be attenuated via tuning the Rpa value in ICP-MS (Hilbig et al., 2017). The response of Fe and Mn signals to Rpa from 0 to 0.02 is shown in **Fig. S6**. The results indicated that Fe and Mn counts were very sensitive to Rpa value in a range from 0.0035 to 0.0084, in which Fe counts decreased linearly from 300000 to 25000, and Mn from 85000,000 to 1000,000.

Furthermore, the LODs of Fe and Mn are 21.2, 30.9, 210 and 0.504, 1.53, 1.56 $\mu g \cdot L^{-1}$ under Rpa 0, 0.005, and 0.01 respectively. Although LODs for Fe and Mn values decreased when the Rpa increased from 0 to 0.01, however it was sufficient for the Fe and Mn detection, since their concentrations are often found above 1 $mg \cdot L^{-1}$ in field porewaters (Gustave et al., 2018b; Wang et al., 2019; Xu et al., 2017). When the ICP-MS was used to measure major elements (e.g. Fe) in low abundance, high Rpa may lead to the unsuccessful determination due to the relatively low LOD, thus is not recommended.

3.3 Comparison of colorimetric and ICP-MS for measuring Fe profiles in field samples

The ICP-MS application on Fe and Mn measurement was further investigated with paddy soil samples. With the method, simultaneous measurement of Fe, Mn, As, P, and S was achieved in the paddy soil samples. The determination coefficients for all the five elements were > 0.99 (**Fig. S7**). The LODs for As, P and S were 0.490, 7.76,

and 60.2 μg·L^{-1}, respectively, which agrees well with previous reports where As, P and S were measured with the ICP-MS (Persson et al., 2009; Yuan et al., 2019). Most studies on porewater Fe used colorimetric analysis for Fe quantification (Arsic et al., 2018; Bennett et al., 2012b). To compare our method with the colorimetric method, two porewater samples were measured using each method.

The Fe profile measured by the ICP-MS with different Rpa values is shown in **Fig. 1**. ICP-MS method with Rpa 0 was unable to measure Fe in soil depth > 25 mm when Fe > 17 mg·L^{-1} in soil porewater because of signal overflow (**Fig. 1A**). Increasing the Rpa from 0 to 0.005 extended the Fe measurement along soil depth from ~ 25 mm to ~ 36 mm (**Fig. 1A&B**), however Rpa 0.005 was still unable to avoid the detector saturation of Fe > 42 mg·L^{-1} in deep soil porewaters (**Fig. 1B**). **Fig. 1C** shows Fe profile could only be measured after the Rpa value was adjusted to 0.01 with Fe ≤ 70 mg·L^{-1}. Similarly to Fe, Rpa 0.005 or 0.01 allowed Mn measurement when Mn ≤ 3.8 mg·L^{-1} in soil porewaters (**Fig. S9**). Although the upper limit was altered with different Rpa values, the Fe and Mn profiles were identical in top soils (0 - 25mm) (**Fig. 1 A-C**, **Fig. S9**).

The porewater samples collected from the same location were also measured by the colorimetric method (**Fig. 1D**). Both colorimetric and ICP-MS methods gave similar results of Fe profiles (p > 0.05). However, Fe concentration measured by the colorimetric method was slightly higher than that obtained by the ICP-MS method. The higher Fe values obtained by the colorimetric method could be attributed to the

interference from other cations (e.g. Mn, calcium, zinc) in the porewater (Hatat-Fraile and Barbeau, 2019; Miranda et al., 2016). Therefore, Fe concentrations might have been overestimated as was reported in previous studies (Braunschweig et al., 2012; Miranda et al., 2016).

3.4 Profiling of total As, Fe, Mn, P and S across SWI

Using the ICP-MS coupled with IPI samplers, we were able to simultaneously measure Fe, Mn, As, P, and S at the mm-scale co-distributions of those elements (**Fig. 2**, relative standard deviation < 8%). As shown in **Fig. 2**, the Fe remained at low concentrations in surface water and top-soil porewater, but increased sharply from 9 mm (1.5 $mg \cdot L^{-1}$) below SWI and reached up to 70 $mg \cdot L^{-1}$ in 50 mm deep soils. Similar trends were observed for Mn, As, and P, which generally increased with depth. The similar vertical changes of Mn, As, P with Fe agree well with their tightly coupling in soils induced by dissimilatory Fe reducing bacteria (Arsic et al., 2018; Ma et al., 2017; Xu et al., 2017). At the 2 - 10 mm zone below SWI, a P pit was observed, which could be attributed to two reasons. First, unlike Fe, Mn, and As, P in surface water remained a relatively high concentration (~ 100 $\mu g \cdot L^{-1}$), which indicated a constant P source existing in the surface water. This part of P is believed to have been released from dead algae degradation (Jarvie et al., 2008). Second, the dissolved P in surface water was trapped by the Fe oxides formed in SWI, where O_2 diffused from surface water reacted with ferrous ions from deep soil (Ajmal et al., 2018; Rietra et al.,

2001).

The S behavior was distinct from Fe, Mn, P, and As (**Fig. 2**). The concentrations of S were high at flooded water and dropped with depth. Sulfur is believed to exist as S(VI) in oxic conditions (Wu et al., 2016), and biotic S(VI) reduction occurs when the redox potential in soils dropped to a highly reducing condition (after easily used electron acceptors were consumed, like O_2, nitrate, Mn and Fe oxides) (Borch et al., 2010). The subsurface decrease of S is therefore presumably caused by S(VI) reducing bacteria in anoxic soils (Pester et al., 2012), which transformed mobile S(VI) to insoluble S(-II) minerals (e.g. FeS, FeS_2) (Wu et al., 2016).

To the best of our knowledge, there is no reported analytical method that can simultaneously measure major and trace elements in the redox gradient zone across SWI. Traditionally, a large volume of subsamples are required to measure Fe, Mn and P by colorimetric methods or ICP-OES (Arsic et al., 2018; Rietra et al., 2001; Serrat, 1998; Wang et al., 2019; Yi et al., 2019), S by IC (Keller-Lehmann et al., 2006), and most traces (e.g. As and antimony) by ICP-MS (Gustave et al., 2018a; Gustave et al., 2019). It is obviously beneficial for studies on element biogeochemical cycles when all the elements can be measured in one injection. The ICP-MS based method dramatically reduces the time consumption for multi-element, thus significantly increases the measurement throughput. The method can also be coupled with other HR samplers, for example, DET and HR peeper.

382 **3.5 As, P, and S species measurement with IC-ICP-MS**

383 The As, P, and S species vary along SWI and determine their environmental fates. In
384 this study, simultaneous detection of four As, two P, and two S species in solution and
385 anoxic soil porewater was achieved with the NH_4HCO_3 as the mobile phase (**Fig. 3**).
386 The retention times were 6.6, 7.5, 3.2, 3.9, 6.0, 10, 3.2, and 8.8 min for P(V), P(III),
387 DMA, As(III), MMA, As(V), S(-II), and S(VI) respectively. The separation of four As
388 species agrees well with previous work using the same chromatographic conditions
389 (Suzuki et al., 2009). The results also demonstrated NH_4HCO_3 mobile phase can be
390 extended to measure P and S species. The determination coefficients for all the three
391 elements are > 0.96 (**Fig. S8**).

392 When applied to soil porewater, 2 As (As(III,V)), 1 P (P(V)), and 2 S (S(-II, VI))
393 species were detected (**Fig. 3**). Arsenite, P(V), and S(-II) (> 70%) represent the
394 dominant As, P and S in soil porewater, respectively. These results agree well with
395 previous reports from multiple soils when the HPLC-ICP-MS, IC or colorimetric
396 methods were used (Chen et al., 2019; Han et al., 2018; Xu et al., 2017). Besides, a
397 susceptible P peak was detected in both solution and porewater with a retention time
398 of 200 s (**Fig. 3**). The retention time is very close to the column dead time for the
399 IC-ICP-MS. which indicates this compound may be cations or small molecules.
400 Among the P species found in environmental samples, phosphine was the only one
401 with neutral in charge, but it is only found in highly reducing environments (Han et al.,

2002), thus can be excluded. Therefore, we extrapolate the P peak at 200 s is likely an interference, such as $^{47}Ti^{+}$, which has the same mass-to-charge ratio of $^{47}PO^{+}$.

Many types of mobile phases were designed to measure the P, S, or As species (**Table 1**). Among the typical mobile phases, the carbonate-based mobile phase (NH_4HCO_3) is better than the others due to its capability to separate the common species of As, P, and S in 10 min. Other chemicals were not suited for various reasons. The P or S containing compounds, like K_2SO_4, 1-butanesulfonic acid, 1-hexanesulfonic acid and $NH_4H_2PO_4$, (Branch et al., 1989; Hirata and Toshimitsu, 2007; Paik et al., 2010) were first excluded because of their interferences with P and S measurement. Nitrate-based mobile phase, such as HNO_3 and NH_4NO_3, (Jackson and Bertsch, 2001; Paik et al., 2010) can be used to separate P and S species, but its elution strength is weaker than that of CO_3^{2-}, which must be used in strong acid condition to shorten the retention time (Jackson and Bertsch, 2001), or in neutral condition with very long running time (Vriens et al., 2014). The acidic condition is not ideal for S(-II) detection, because it encourages gaseous H_2S formation. The alkali hydroxyl-based mobile phase is widely used to As and S species measurement by IC-ICP-MS (Divjak and Goessler, 1999; Jackson and Bertsch, 2001). However, the hydroxyl-based mobile phase often contains alkali metal cations, like sodium, which can clog the plasma torch, sampling corn, or skimmer corn by the inorganic salts deposition. Thus, NH_4HCO_3 is the best choice to develop a mobile phase for simultaneously separating P, S, and As species.

423 The NH_4HCO_3 mobile phase pH (10) is appropriate to form P, S, and As species
424 of different charges (Divjak and Goessler, 1999; McDowell et al., 2004; Reid et al.,
425 2020). However, the alkali condition may cause Fe oxides precipitation when the
426 mobile phase mixed with the high Fe porewater. The precipitates could bind with the
427 anions, and potentially interfere with the testing and cause clog in the analytical
428 column. Thus, EDTA was pre-added into samples before sample injection to the IC.
429 EDTA could mitigate the precipitation of metal ions within a wide range of pH
430 (Almkvist et al., 2013; Gallagher et al., 2001; Samanta and Clifford, 2006). With
431 EDTA addition, no metal oxides precipitation was observed during IC-ICP-MS
432 measurement.

433

434 **3.6 Profiling of P, S and As species across SWI**

435 The optimized IC-ICP-MS method was further verified with soil porewater collected
436 by SWI profilers. The vertical changes of As(III), As(V), P(V), S(-II) and S(IV) are
437 depicted in **Fig. 4**. Among the species, As(III), As(V), P(V) and S(-II) were low in top
438 layers, and increased gradually from 7.9, 0.70, 60 $\mu g \cdot L^{-1}$ and 1.6 $mg \cdot L^{-1}$ at ~ 13 mm
439 below SWI to over 200, 50, 200 $\mu g \cdot L^{-1}$ and 15 $mg \cdot L^{-1}$ in deep soils respectively. The
440 S(VI) change was consistent with the total S, which decreased along the soil depth
441 (**Fig. 4**). The As, P and S trends agree with their fates in flooded soils, and the results
442 revealed by other methods (Arsic et al., 2018; Han et al., 2018; Mcadams et al., 2016;
443 Robertson et al., 2008).

444 According to the element profiles, we noticed that there was an overlap between
445 dissolved Fe and S(-II) in pretty high concentrations at >15 mm below SWI (**Fig.**
446 **2&4**). Ferrous ions are the main form of dissolved Fe in reducing condition, and not
447 supposed to co-exist with S(-II) in aqueous phase in theory because they form
448 insoluble FeS (Rickard, 2006). However, the co-existence of ferrous ions and S(-II)
449 were frequently reported in many field samples (Pagès et al., 2011; Robertson et al.,
450 2008; Robertson et al., 2009) and we speculate that the ferrous ions may be chelated
451 with dissolved organic matters and stabilized in aqueous phase.

452 Although the redox-sensitive elements speciation has received much attention,
453 most analytical methods for those species were developed for single element only
454 (Divjak and Goessler, 1999; Han et al., 2018; Jackson and Bertsch, 2001). In
455 comparison with those methods, the optimized method in the current study has higher
456 measurement throughput, which can simultaneously measure As, P and S species
457 within 10 min in a single run. The method is well suited for coupling with HR
458 samplers to map multi-species profiles across SWI.

459

460 **4. Conclusions**

461 Simultaneous measurement of multi-element (Fe, Mn, As, P, S) and multi-species
462 (As(III), As(V), MMA, DMA, P(III), P(V), S(-II) and S(VI)), in volume-limited
463 samples (~ 100 μL level), was achieved with the ICP-MS and IC-ICP-MS analysis.

The method demonstrated both high sensitivity (μg·L^{-1} level) and high throughput. Combining the optimized analytical methods and a HR porewater sampler (i.e. IPI), we successfully measured the mm-scale co-distributions of multi-element (Fe, Mn, As, P and S) and multi-species (As(III), As(V), P(V), S(-II) and S(VI)) along SWI. With rapid measurement of multiple parameters from limited samples, the optimized analytical methods enable researchers to measure aqueous chemistry (including pure solution, surface water, porewater and groundwater) at high throughput. Moreover, the optimized analytical methods are very well suited for limited samples analysis in HR samplers (e.g. IPI, DET and peeper). The combination of the method and HR samplers can provide as much as possible aqueous parameters, thus facilitate studies of elements cycling in micro interfaces (e.g. SWI) of soils, sediments and other aqueous environments.

Acknowledgments

This work was supported by the National Science Foundation of China (Nos. 41977320, 41571305), Key Programme Special Fund of XJTLU (No. KSF-A-20). The authors acknowledge the kind help of Fuyuan Liu for the 3D printing model design. The authors also acknowledge the kind help of Yi-Li Cheng, Xiao Zhou, Xiao-Yan Zhang, and Liang-Ping Long for their support in instrumental analysis.

Appendix A. Supplementary data

Supplementary data associated with this article can be found in the online version at xxxxxx.

References

Ajmal, Z., Muhmood, A., Usman, M., Kizito, S., Lu, J., Dong, R., et al., 2018. Phosphate removal from aqueous solution using iron oxides: Adsorption, desorption and regeneration characteristics. J. Colloid Interf. Sci. 528:145-155.

Almkvist, G., Hocker, E., Sahlstedt, M., Museums, S.M., 2013. Iron removal from waterlogged wood. Swedish University of Agricultural Sciences. SLU Repro, Uppsala.

Arsic, M., Teasdale, P.R., Welsh, D.T., Johnston, S.G., Burton, E.D., Hockmann, K., et al., 2018. Diffusive gradients in thin films (DGT) reveals antimony and arsenic mobility differs in a contaminated wetland sediment during an oxic-anoxic transition. Environ. Sci. Technol. 52:1118-1127.

Bennett, W.W., Teasdale, P.R., Panther, J.G., Welsh, D.T., Zhao, H., Jolley, D.F., 2012a. Investigating arsenic speciation and mobilization in sediments with DGT and DET: a mesocosm evaluation of oxic-anoxic transitions. Environ. Sci. Technol. 46:3981-3989.

Bennett, W.W., Teasdale, P.R., Welsh, D.T., Panther, J.G., Jolley, D.F., 2012b. Optimization of colorimetric DET technique for the in situ, two-dimensional measurement of iron (II) distributions in sediment porewaters. Talanta 88:490-495.

Borch, T., Kretzschmar, R., Kappler, A., Cappellen, P.V., Gindervogel, M., Voegelin, A., et al., 2010. Biogeochemical redox processes and their impact on contaminant dynamics. Environ. Sci. Technol. 44:15-23.

507 Bottrell, S.H., Mortimer, R.J., Spence, M., Krom, M.D., Clark, J.M., Chapman, P.J., 2007. Insights into
508 redox cycling of sulfur and iron in peatlands using high-resolution diffusive equilibrium thin film
509 (DET) gel probe sampling. Chem. Geol. 244:409-420.

510 Branch, S., Bancroft, K., Ebdon, L., O'Neill, P., 1989. The determination of arsenic species by coupled
511 high-performance liquid chromatography-atomic spectrometry. Anal. Proc. 26:73-75.

512 Braunschweig, J., Bosch, J., Heister, K., Kuebeck, C., Meckenstock, R.U., 2012. Reevaluation of
513 colorimetric iron determination methods commonly used in geomicrobiology. J. Microbiol. Meth.
514 89:41-48.

515 Chen, C., Li, L., Huang, K., Zhang, J., Xie, W.Y., Lu, Y., et al., 2019. Sulfate-reducing bacteria and
516 methanogens are involved in arsenic methylation and demethylation in paddy soils. ISME J.
517 13:2523-2535.

518 Chen, Z., He, W., Beer, M., Megharaj, M., Naidu, R., 2009. Speciation of glyphosate, phosphate and
519 aminomethylphosphonic acid in soil extracts by ion chromatography with inductively coupled
520 plasma mass spectrometry with an octopole reaction system. Talanta 78:852-856.

521 Cheng, G., He, M., Peng, H., Hu, B., 2012. Dithizone modified magnetic nanoparticles for fast and
522 selective solid phase extraction of trace elements in environmental and biological samples prior to
523 their determination by ICP-OES. Talanta 88:507-515.

524 Cotta, A.J.B., Enzweiler, J., 2009. Quantification of major and trace elements in water samples by
525 ICP-MS and collision cell to attenuate Ar and Cl-based polyatomic ions. J. Anal. Atom. Spectrom.
526 24:1406-1413.

527 Davison, W., Zhang, H., 1994. In situ speciation measurements of trace components in natural waters
528 using thin-film gels. Nature 367:546.

529 Di, X., Wei, W., Shiming, D., Qin, S., Chaosheng, Z., 2012. A high-resolution dialysis technique for
530 rapid determination of dissolved reactive phosphate and ferrous iron in pore water of sediments.
531 Sci. Total Environ. 421-422:245-252.

532 Ding, S., Wang, Y., Wang, D., Li, Y.Y., Gong, M., Zhang, C., 2016. In situ, high-resolution evidence for
533 iron-coupled mobilization of phosphorus in sediments. Sci. Rep. 6:24341.

534 Divjak, B., Goessler, W., 1999. Ion chromatographic separation of sulfur-containing inorganic anions
535 with an ICP–MS as element-specific detector. J. Chromatogr. A 844:161-169.

536 Divjak, B., Novič, M., Goessler, W., 1999. Determination of bromide, bromate and other anions with
537 ion chromatography and an inductively coupled plasma mass spectrometer as element-specific
538 detector. J. Chromatogr. A 862:39-47.

539 Dočekalová, H., Clarisse, O., Salomon, S., Wartel, M., 2002. Use of constrained DET probe for a
540 high-resolution determination of metals and anions distribution in the sediment pore water. Talanta
541 57:145-155.

542 Fang, W., Williams, P.N., Fang, X., Amoah-Antwi, C., Yin, D., Li, G., et al., 2018. Field-scale
543 heterogeneity and geochemical regulation of arsenic, iron, lead, and sulphur bioavailability in
544 paddy soil. Environ. Sci. Technol. 52:12098–12107.

545 Frenzel, P., Rothfuss, F., Conrad, R., 1992. Oxygen profiles and methane turnover in a flooded rice
546 microcosm. Biol. Fert. Soils 14:84-89.

547 Gallagher, P.A., Schwegel, C.A., Wei, X., Creed, J.T., 2001. Speciation and preservation of inorganic
548 arsenic in drinking water sources using EDTA with IC separation and ICP-MS detection. J.
549 Environ. Monitor. 3:371-376.

550 Gao, L., Gao, B., Zhou, H., Xu, D., Wang, Q., Yin, S., 2016. Assessing the remobilization of antimony
551 in sediments by DGT: a case study in a tributary of the Three Gorges Reservoir. Environ. Pollut.
552 214:600-607.

553 Gao, Y., Leermakers, M., Elskens, M., Billon, G., Ouddane, B., Fischer, J.-C., et al., 2007. High
554 resolution profiles of thallium, manganese and iron assessed by DET and DGT techniques in
555 riverine sediment pore waters. Sci. Total Environ. 373:526-533.

556 Gao, Y., Leermakers, M., Gabelle, C., Divis, P., Billon, G., Ouddane, B., et al., 2006. High-resolution
557 profiles of trace metals in the pore waters of riverine sediment assessed by DET and DGT. Sci.
558 Total Environ. 362:266-277.

559 Guan, D.X., Williams, P.N., Luo, J., Zheng, J.L., Xu, H.C., Cai, C., et al., 2015. Novel precipitated
560 zirconia-based DGT technique for high-resolution imaging of oxyanions in waters and sediments.
561 Environ. Sci. Technol. 49:3653-3661.

562 Gustave, W., Yuan, Z.F., Sekar, R., Chang, H.C., Zhang, J., Wells, M., et al., 2018a. Arsenic mitigation
563 in paddy soils by using microbial fuel cells. Environ. Pollut. 238:647-655.

564 Gustave, W., Yuan, Z.F., Sekar, R., Ren, Y.X., Chang, H.C., Liu, J.Y., et al., 2018b. The change in biotic
565 and abiotic soil components influenced by paddy soil microbial fuel cells loaded with various
566 resistances. J. Soil. Sediment. 19:106-115.

567 Gustave, W., Yuan, Z.F., Sekar, R., Ren, Y.X., Liu, J.Y., Zhang, J., et al., 2019. Soil organic matter
568 amount determines the behavior of iron and arsenic in paddy soil with microbial fuel cells.
569 Chemosphere 237:124459.

570 Han, C., Williams, P.N., Ren, J., Wang, Z., Fang, X., Xu, D., et al., 2018. In situ sampling and
571 speciation method for measuring dissolved phosphite at ultratrace concentrations in the natural
572 environment. Water Res. 137:281-289.

573 Han, S., Zhuang, Y., Zhang, H., Wang, Z., Yang, J., 2002. Phosphine and methane generation by the
574 addition of organic compounds containing carbon–phosphorus bonds into incubated soil.
575 Chemosphere 49:651-657.

576 Hatat-Fraile, M., Barbeau, B., 2019. Performance of colorimetric methods for the analysis of low levels
577 of manganese in water. Talanta 194:786-794.

578 Hilbig, H., Huber, M., Gmell, A., Heinz, D., 2017. Determination of heavy metals in a highly porous
579 sorptive filter material of road runoff treatment systems with LA-ICP-MS. Water Air Soil Poll.
580 228:331.

581 Hirata, S., Toshimitsu, H., 2007. Determination of arsenic species and arsenosugars in marine samples
582 by HPLC‐ICP‐MS. Appl. Organomet. Chem. 21:447-454.

583 Huo, S., Zhang, J., Yeager, K.M., Xi, B., Qin, Y., He, Z., et al., 2015. Mobility and sulfidization of
584 heavy metals in sediments of a shallow eutrophic lake, Lake Taihu, China. J. Environ. Sci.
585 31:1-11.

586 Jackson, B.P., Bertsch, P.M., 2001. Determination of arsenic speciation in poultry wastes by
587 IC-ICP-MS. Environ. Sci. Technol. 35:4868-4873.

588 Jarvie, H.P., Mortimer, R.J., Palmer-Felgate, E.J., Quinton, K.S., Harman, S.A., Carbo, P., 2008.
589 Measurement of soluble reactive phosphorus concentration profiles and fluxes in river-bed
590 sediments using DET gel probes. J. Hydrol. 350:261-273.

591 Jones, M.E., Nico, P.S., Ying, S., Regier, T., Thieme, J., Keiluweit, M., 2018. Manganese-driven carbon
592 oxidation at oxic–anoxic interfaces. Environ. Sci. Technol. 52:12349-12357.

593 Keller-Lehmann, B., Corrie, S., Ravn, R., Yuan, Z., Keller, J., 2006. Preservation and simultaneous
594 analysis of relevant soluble sulfur species in sewage samples. Proceedings of the Second
595 International IWA Conference on Sewer Operation and Maintenance 26:28.

596 Laskov, C., Herzog, C., Lewandowski, J., Hupfer, M., 2007. Miniaturized photometrical methods for
597 the rapid analysis of phosphate, ammonium, ferrous iron, and sulfate in pore water of freshwater
598 sediments. Limnol. Oceanogr.: Methods 5:63-71.

599 Lin, L.-Y., Jiang, S.-J., 2009. Determination of sulfur compounds in water samples by ion
600 chromatography dynamic reaction cell inductively coupled plasma mass spectrometry. J. Chin.
601 Chem. Soc. 56:967-973.

602 Lumbaque, E.C., da Silva, B.A., Böck, F.C., Helfer, G.A., Ferrão, M.F., Sirtori, C., 2019. Total
603 dissolved iron and hydrogen peroxide determination using the PhotoMetrixPRO application: A
604 portable colorimetric analysis tool for controlling important conditions in the solar photo-Fenton
605 process. J. Hazard. Mater. 378:120740.

606 Ma, W.W., Zhu, M.X., Yang, G.P., Li, T., 2017. In situ, high-resolution DGT measurements of
607 dissolved sulfide, iron and phosphorus in sediments of the East China Sea: Insights into
608 phosphorus mobilization and microbial iron reduction. Mar. Pollut. Bull. 124:400-410.

609 Mcadams, B.C., Adams, R.M., Arnold, W.A., Chin, Y.P., 2016. Novel insights into the distribution of
610 reduced sulfur species in prairie pothole wetland pore waters provided by bismuth film electrodes.
611 Environ. Sci. Technol. Lett. 3:104-109.

612 McDowell, M.M., Ivey, M.M., Lee, M.E., Firpo, V.V., Salmassi, T.M., Khachikian, C.S., et al., 2004.
613 Detection of hypophosphite, phosphite, and orthophosphate in natural geothermal water by ion
614 chromatography. J. Chromatogr. A 1039:105-111.

615 Miranda, J.L., Mesquita, R.B., Nunes, A., Rangel, M., Rangel, A.O., 2016. Iron speciation in natural
616 waters by sequential injection analysis with a hexadentate 3-hydroxy-4-pyridinone chelator as
617 chromogenic agent. Talanta 148:633-640.

618 Monbet, P., McKelvie, I.D., Worsfold, P.J., 2008. Combined gel probes for the in situ determination of
619 dissolved reactive phosphorus in porewaters and characterization of sediment reactivity. Environ.
620 Sci. Technol. 42:5112-5117.

621 Morton, S.C., Glindemann, D., Wang, X., Niu, X., Edwards, M., 2005. Analysis of reduced phosphorus
622 in samples of environmental interest. Environ. Sci. Technol. 39:4369-4376.

623 Motelica-Heino, M., Naylor, C., Zhang, H., Davison, W., 2003. Simultaneous release of metals and
624 sulfide in lacustrine sediment. Environ. Sci. Technol. 37:4374-4381.

625 Pagès, A., Teasdale, P.R., Robertson, D., Bennett, W.W., Schäfer, J., Welsh, D.T., 2011. Representative
626 measurement of two-dimensional reactive phosphate distributions and co-distributed iron (II) and
627 sulfide in seagrass sediment porewaters. Chemosphere 85:1256-1261.

628 Paik, M.K., Kim, M.J., Kim, W.I., Yoo, J.H., Park, B.J., Im, G.J., et al., 2010. Determination of arsenic
629 species in polished rice using a methanol-water digestion method. J. Korean Soc. Appl. Biol.
630 Chem. 53:634-638.

631 Peng, C., Bryce, C., Sundman, A., Kappler, A., 2019. Cryptic cycling of complexes containing Fe (III)
632 and organic matter by phototrophic Fe (II)-oxidizing bacteria. Appl. Environ. Microbiol.
633 85:e02826-02818.

634 Persson, D.P., Hansen, T.H., Laursen, K.H., Schjoerring, J.K., Husted, S., 2009. Simultaneous iron,
635 zinc, sulfur and phosphorus speciation analysis of barley grain tissues using SEC-ICP-MS and
636 IP-ICP-MS. Metallomics 1:418-426.

637 Pester, M., Knorr, K.H., Friedrich, M.W., Wagner, M., Loy, A., 2012. Sulfate-reducing microorganisms
638 in wetlands–fameless actors in carbon cycling and climate change. Front. Microbiol. 3:72.

639 Pi, K., Wang, Y., Postma, D., Teng, M., Su, C., Xie, X., 2018. Vertical variability of arsenic
640 concentrations under the control of iron-sulfur-arsenic interactions in reducing aquifer systems. J.
641 Hydrol. 561:200-210.

642 Ratering, S., Schnell, S., 2001. Nitrate - dependent iron (II) oxidation in paddy soil. Environ.
643 Microbiol. 3:100-109.

644 Reid, M.S., Hoy, K.S., Schofield, J.R.M., Uppal, J.S., Lin, Y., Lu, X., et al., 2020. Arsenic speciation
645 analysis: A review with an emphasis on chromatographic separations. TrAC Trend. Anal. Chem.
646 123:115770.

647 Reynolds, B., Stevens, P., Hughes, S., Brittain, S., 2004. Comparison of field techniques for sampling
648 soil solution in an upland peatland. Soil Use Manage. 20:454-456.

649 Rickard, D., 2006. The solubility of FeS. Geochim. Cosmochim. Ac. 70:5779-5789.

650 Rietra, R.P.J.J., Hiemstra, T., Van Riemsdijk, W.H., 2001. Interaction between calcium and phosphate
651 adsorption on goethite. Environ. Sci. Technol. 35:3369-3374.

652 Robertson, D., Teasdale, P.R., Welsh, D.T., 2008. A novel gel‐based technique for the high resolution,
653 two‐dimensional determination of iron (II) and sulfide in sediment. Limnol. Oceanogr-Meth.
654 6:502-512.

655 Robertson, D., Welsh, D.T., Teasdale, P.R., 2009. Investigating biogenic heterogeneity in coastal
656 sediments with two-dimensional measurements of iron (II) and sulfide. Environ. Chem. 6:60-69.

657 Samanta, G., Clifford, D.A., 2006. Preservation and field speciation of inorganic arsenic species in
658 groundwater. Water Qual. Res. J. Can. 41:107-116.

659 Seeberg‐Elverfeldt, J., Schlüter, M., Feseker, T., Kölling, M., 2005. Rhizon sampling of porewaters
660 near the sediment‐water interface of aquatic systems. Limnol. Oceanogr-Meth. 3:361-371.

661 Serrat, F.B., 1998. 3, 3′, 5, 5′-Tetramethylbenzidme for the colorimetric determination of
662 manganese in water. Microchim. Acta 129:77-80.

663 Sun, Q., Ding, S., Zhang, L., Chen, M., Zhang, C., 2017. A millimeter-scale observation of the
664 competitive effect of phosphate on promotion of arsenic mobilization in sediments. Chemosphere
665 180:285.

666 Suzuki, Y., Shimoda, Y., Endo, Y., Hata, A., Yamanaka, K., Endo, G., 2009. Rapid and effective
667 speciation analysis of arsenic compounds in human urine using anion-exchange columns in
668 HPLC-ICP-MS. J. Occup. Health 51:380-385.

669 Tanner, S.D., Baranov, V.I., 1999. A dynamic reaction cell for inductively coupled plasma mass
670 spectrometry (ICP-DRC-MS). II. Reduction of interferences produced within the cell. J. Am. Soc.
671 Mass Spectr. 10:1083-1094.

672 Vriens, B., Ammann, A.A., Hagendorfer, H., Lenz, M., Berg, M., Winkel, L.H.E., 2014. Quantification
673 of methylated selenium, sulfur, and arsenic in the environment. PLoS One 9:e102906-e102906.

674 Wang, M., Tang, Z., Chen, X.P., Wang, X., Zhou, W.X., Tang, Z., et al., 2019. Water management
675 impacts the soil microbial communities and total arsenic and methylated arsenicals in rice grains.
676 Environ. Pollut. 247:736-744.

677 Wen, S., Wu, T., Yang, J., Jiang, X., Zhong, J., 2019. Spatio-temporal variation in nutrient profiles and
678 exchange fluxes at the sediment-water interface in Yuqiao Reservoir, China. Int. J. Environ. Res.
679 Public Health 16:3071.

680 Williams, P.N., Santner, J., Larsen, M., Lehto, N.J., Oburger, E., Wenzel, W., et al., 2014. Localized
681 flux maxima of arsenic, lead, and iron around root apices in flooded lowland rice. Environ. Sci.
682 Technol. 48:8498-8506.

683 Wu, Z., Ren, D., Zhou, H., Hang, G., Li, J., 2016. Sulfate reduction and formation of iron sulfide
684 minerals in nearshore sediments from Qi'ao Island, Pearl River Estuary, Southern China. Quatern.
685 Int. 452:137-147.

686 Xu, D., Wu, W., Ding, S., Sun, Q., Zhang, C., 2012. A high-resolution dialysis technique for rapid
687 determination of dissolved reactive phosphate and ferrous iron in pore water of sediments. Sci.
688 Total Environ. 421:245-252.

689 Xu, X., Chen, C., Wang, P., Kretzschmar, R., Zhao, F.J., 2017. Control of arsenic mobilization in paddy
690 soils by manganese and iron oxides. Environ. Pollut. 231:37-47.

691 Yi, X.Y., Yang, Y.P., Yuan, H.Y., Chen, Z., Duan, G.L., Zhu, Y.G., 2019. Coupling metabolisms of
692 arsenic and iron with humic substances through microorganisms in paddy soil. J. Hazard. Mater.
693 373:591-599.

694 Yin, D.X., Fang, W., Guan, D.X., Williams, P.N., Moreno Jimenez, E., Gao, Y., et al., 2020. Localized
695 intensification of arsenic release within the emergent rice rhizosphere. Environ. Sci. Technol.
696 54:3138-3147.

697 Yuan, Z.F., Gustave, W., Bridge, J., Liang, Y., Sekar, R., Boyle, J., et al., 2019. Tracing the dynamic
698 changes of element profiles by novel soil porewater samplers with ultralow disturbance to soil–
699 water interface. Environ. Sci. Technol. 53:5124-5132.

700 Zhai, H., Wang, L., Hövelmann, J., Qin, L., Zhang, W., Putnis, C.V., 2018. Humic acids limit the
701 precipitation of cadmium and arsenate at the Brushite− Fluid interface. Environ. Sci. Technol.
702 53:194-202.

List of tables

Table 1 Separation of As, P and S species with IC-ICP-MS under different conditions

Mobile phase	pH	Species measured	Tr.§	Ref.
HNO_3	1.3 - 2.6	As(III, V), MMA, DMA	5	(Jackson and Bertsch, 2001)
$C_4H_{10}O_3S$†+ $C_6H_{14}O_3S$‡	3.0	As(V), DMA	5	(Hirata and Toshimitsu, 2007)
	5.1	P(V)	5	(Chen et al., 2009)
NH_4NO_3	7.0	S(IV, VI), thiosulfate	5	(Lin and Jiang, 2009)
	7.5	As(III, V), MMA, DMA, S(VI)	15	(Vriens et al., 2014)
NH_4NO_3+ $NH_4H_2PO_4$	7.2 +8.2	As(III, V), MMA, DMA	15	(Paik et al., 2010)
NH_4HCO_3	10	As(III, V), MMA, DMA	9	(Suzuki et al., 2009)
	10	P(III, V), S(-II, VI)	10	This study
K_2SO_4	10.5	As(III, V), MMA, DMA	7	(Branch et al., 1989)
$(NH_4)_2CO_3$	11.2	As(V), P(V), S(VI)	4	(Divjak et al., 1999)
NaOH	> 12	As(III, V), MMA, DMA	8	(Jackson and Bertsch, 2001)
		S(-II, IV, VI)	8	(Divjak and Goessler, 1999)

§ measurement throughput (min per sample); † 1-butanesulfonic acid; ‡ 1-hexanesulfonic acid; arsenite, As(III); arsenate, As(V); monomethylarsonic, MMA; dimethylarsinic, DMA; hypophosphite, P(I); phosphite, P(III); phosphate, P(V); sulfide, S(-II); sulfite, S(IV); sulfate, S(VI).

List of figures

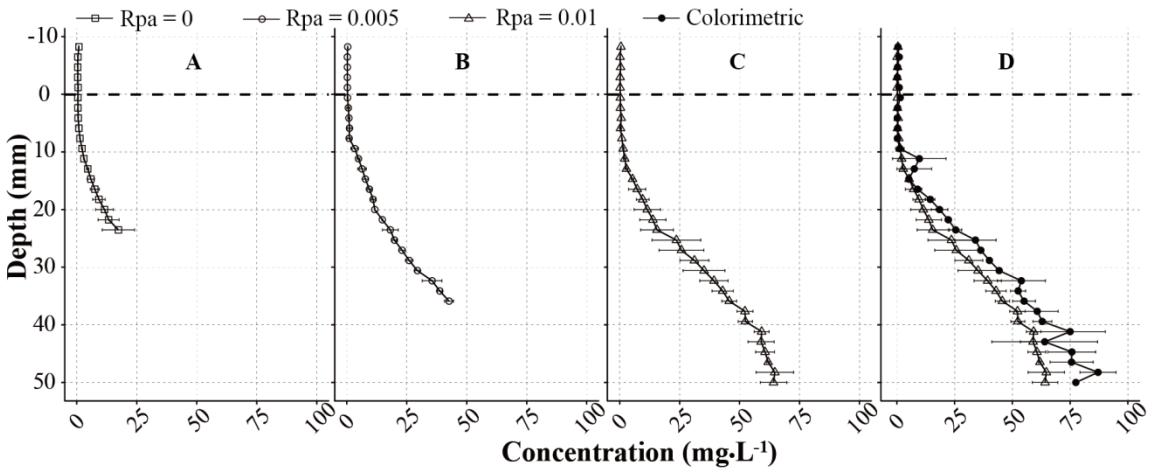

Figure 1 Iron profiles measured by ICP-MS under extended dynamic range mode or colorimetric method (phenanthroline) in Shaoguan (SG) paddy. A-C): Fe profile measurement with ICP-MS method when 'rejection parameter a' (Rpa) = 0, 0.005 and 0.01 respectively; D) Fe profile measured by colorimetric and ICP-MS method (Rpa = 0.01). The triangle symbols in C) and D) share the same dataset. The error bar is the standard deviation (n = 2). The black dashed line at depth zero is the soil-water interface.

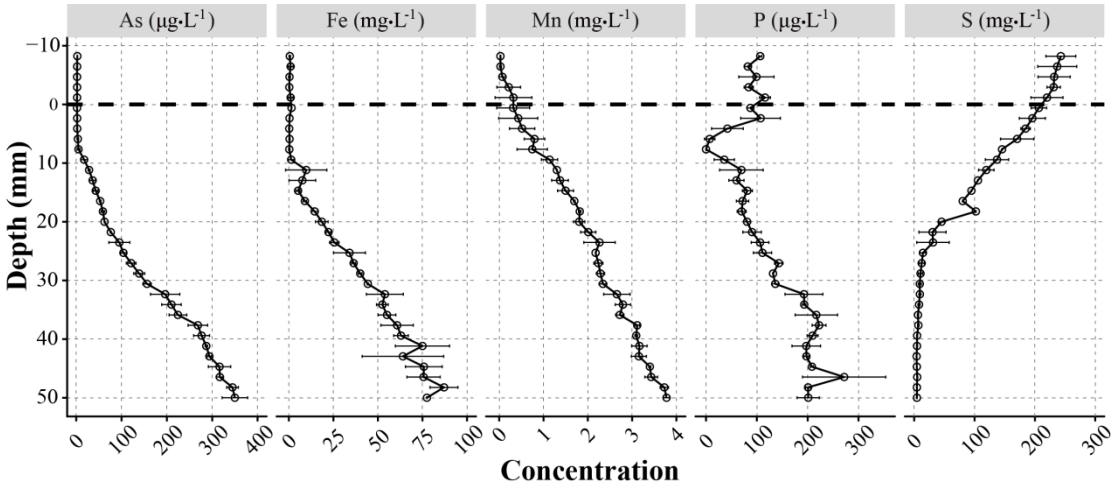

719

720 **Figure 2** Mapping of As, Fe, Mn, P, and S profiles in Shaoguan (SG) paddy with
721 ICP-MS.

722

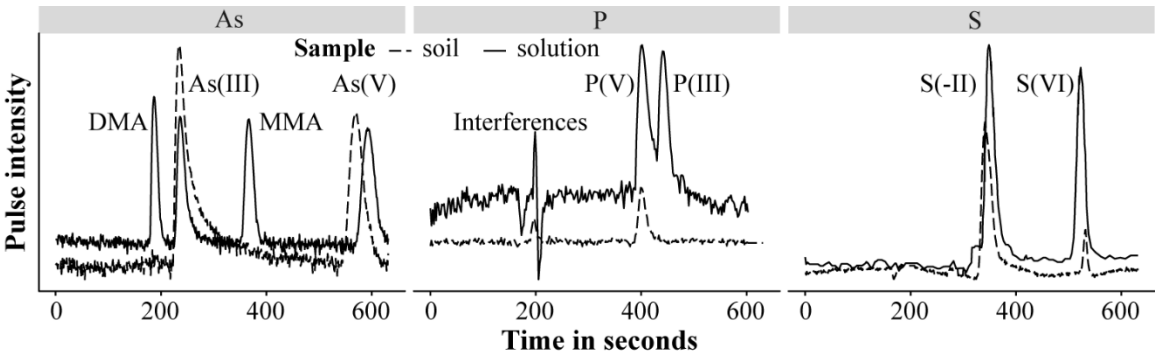

723

724 **Figure 3** Arsenic (As), phosphorus (P), and sulfur (S) species detected by IC-ICP-MS.
725 The samples include soil porewater and solution. The solution was prepared in neutral
726 conditions (pH 7; 100 $\mu g \cdot L^{-1}$ phosphite (P(III)), phosphate (P(V)), arsenite (As(III)),
727 arsenate (As(V)), monomethylarsonic (MMA) and dimethylarsinic (DMA); 1 $mg \cdot L^{-1}$
728 sulfide (S(-II)) and sulfate (S(VI))).

729

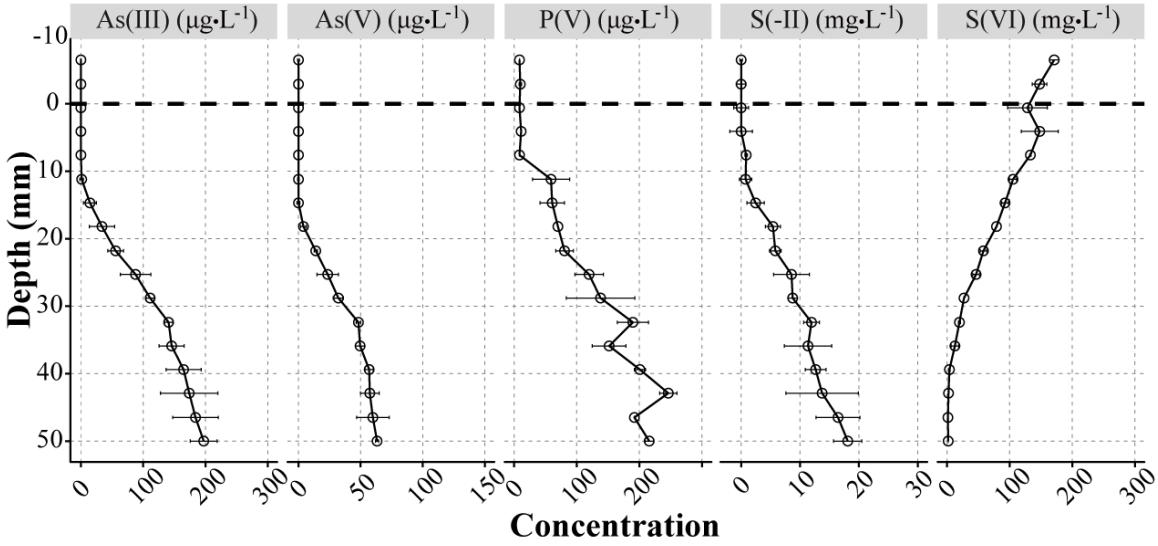

730

731 **Figure 4** Profiles of P, S and As species in SG paddy measured by SWI profiler and
732 NH_4HCO_3 eluent.

733

Simultaneous measurement of aqueous redox-sensitive elements and their species across the soil-water interface

Zhao-Feng Yuan [1, 2, 3], Williamson Gustave [1, 2, 4], Raju Sekar [5], Jonathan Bridge [6], Jia-Yue Wang [1], Wei-Jia Feng [1], Bin Guo [7 *] and Zheng Chen [1 *]

[1] Department of Health and Environmental Sciences, Xi'an Jiaotong-Liverpool University, 111 Ren'ai Road, Suzhou, Jiangsu 215123, China. E-mail: ebiogeochem@outlook.com

[2] Department of Environmental Science, University of Liverpool, Brownlow Hill, Liverpool L69 7ZX, UK.

[3] Department of Plant Science, Tarim University, Alaer, Xinjiang 843300, China.

[4] Chemistry, Environmental & Life Sciences, University of The Bahamas, New Providence, Nassau, The Bahamas.

[5] Department of Biological Sciences, Xi'an Jiaotong-Liverpool University, 111 Ren'ai Road, Suzhou, Jiangsu 215123, China.

[6] Department of Natural and Built Environment, Sheffield Hallam University, Howard St, Sheffield S1 1WB, UK.

[7] Institute of Environment, Resource, Soil and Fertilizer, Zhejiang Academy of Agricultural Sciences, Hangzhou, 310021, China.

Received 31 July 2020

Revised 31 August 2020

---

* **Corresponding author.** E-mail: ebiogeochem@outlook.com (Zheng Chen); Email: ndgb@163.com (Bin Guo)

Table S1 The selected physicochemical characteristics of Shaoguan (SG) paddy soils used in this study

Location	Soil type	As (mg kg^{-1})	Fe (g kg^{-1})	P (mg kg^{-1})	S (%)	Mn (g kg^{-1})
SG	loam	146	227	40.0	0.40	1.50

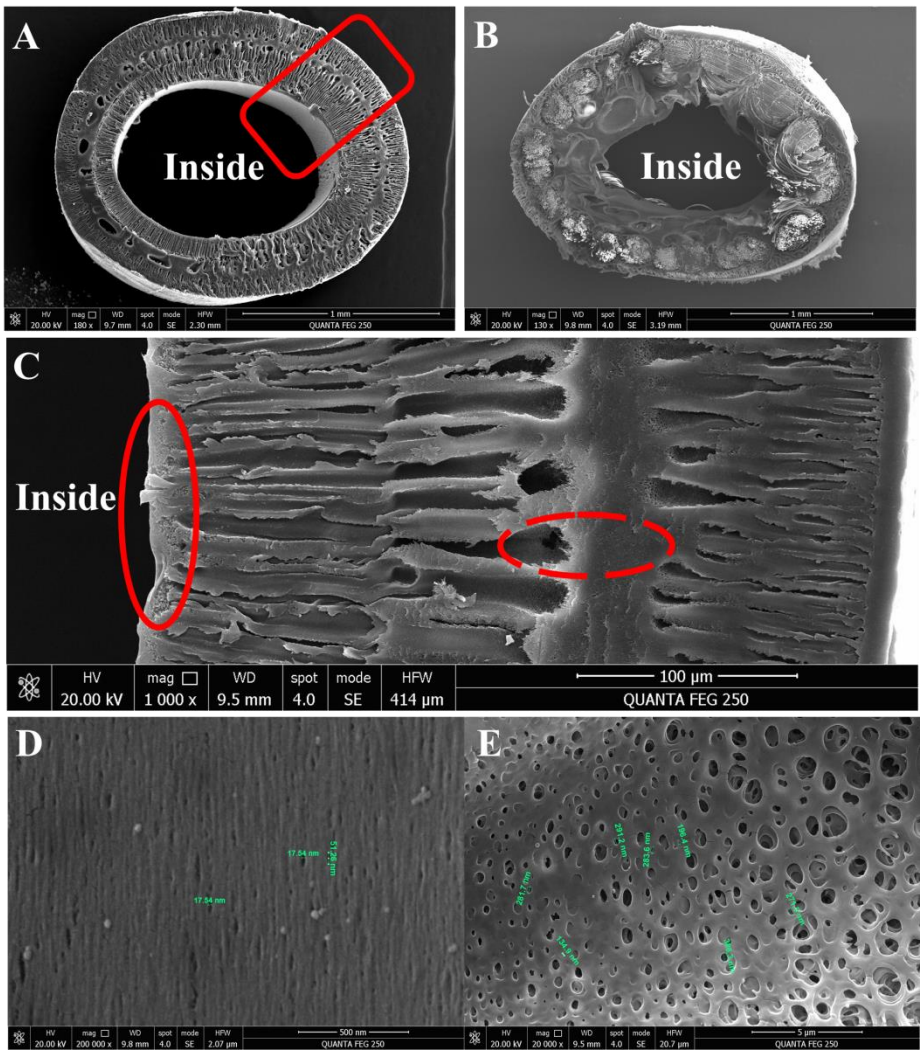

Figure S1 Pore size of the membrane determined by SEM. A-B) vertical section of the novel modified polyethersulfone membrane and the old polyvinylidene fluoride membrane respectively, the red frame is the selected region for further magnification in C); and solid and dashed eclipses in C) are the selected region for pore size determination in D) and E) respectively. The pore size of the novel membrane for analytes is determined by its inside-layer with a pore size of ~ 20 nm.

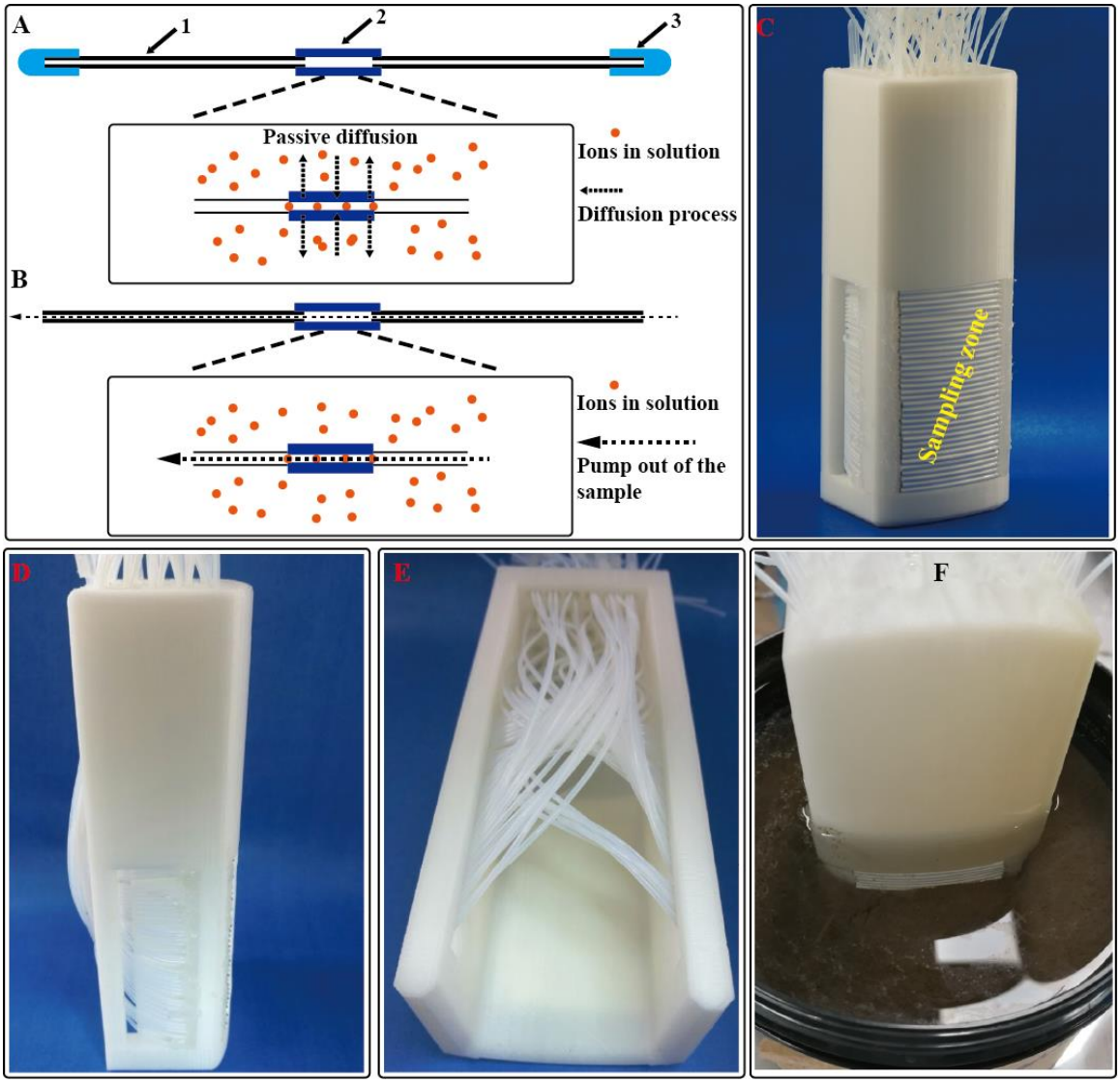

Figure S2 Schematic diagram of *In-situ* Porewater Iterative (IPI) sampler. A) elements ions diffuse through the hollow fiber membrane; B) the solution inside the hollow fiber membrane tube is pumped out from the tube and collected; C) photo of IPI sampler array (SWI profiler), SWI profiler consists of 34 IPI samplers, which are assembled horizontally in the plastic holder; D) photo of IPI sampler (side); E) photo of IPI sampler (back and bottom); F) photo of SWI profiler deployed in soils. Note (A): 1. pipe; 2. hollow fiber membrane tube; 3. silicon cap.

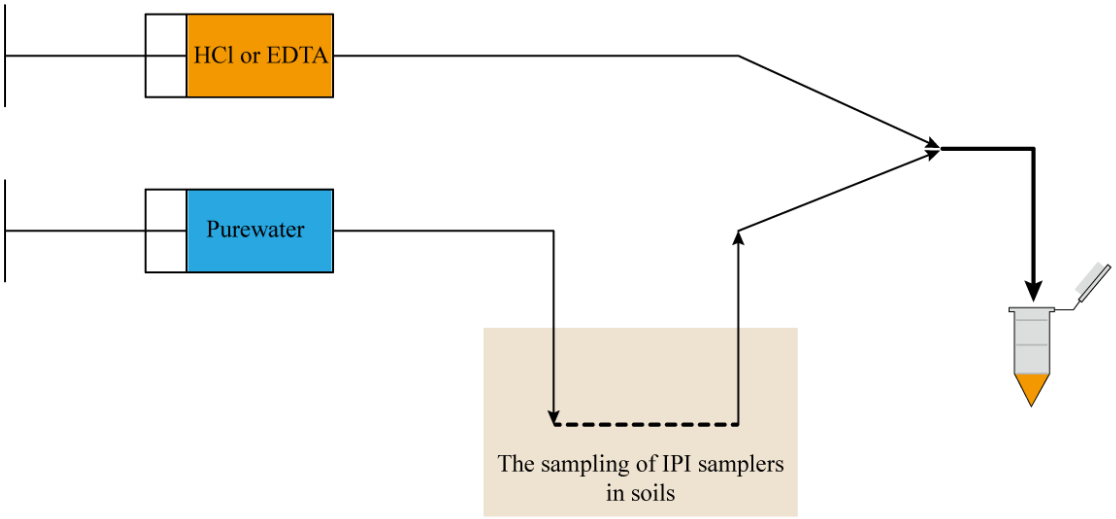

776

777 **Figure S3** The sampling process of IPI samplers in saturated soils. After the sampling
778 of the IPI sampler reaches equilibrium, the sample is collected powered by an
779 injection pump with pure water, and online mixed with the HCl or EDTA solution to
780 preserve the sample. The arrows indicate the flow direction.

781

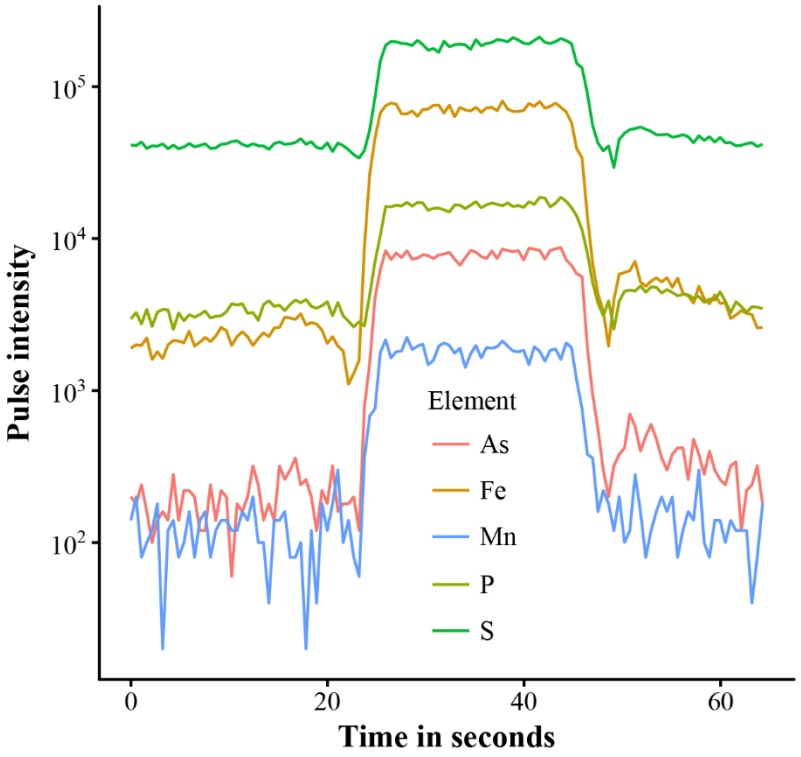

782

783 **Figure S4** Measurement of As, Fe, Mn, P, and S in 50 μL solution by data only
784 analysis in ICP-MS. The solution was prepared in 2% HNO_3, with 10 $\mu g \cdot L^{-1}$ As and
785 Mn, 100 $\mu g \cdot L^{-1}$ P, and 1.0 $mg \cdot L^{-1}$ Fe and S.

786

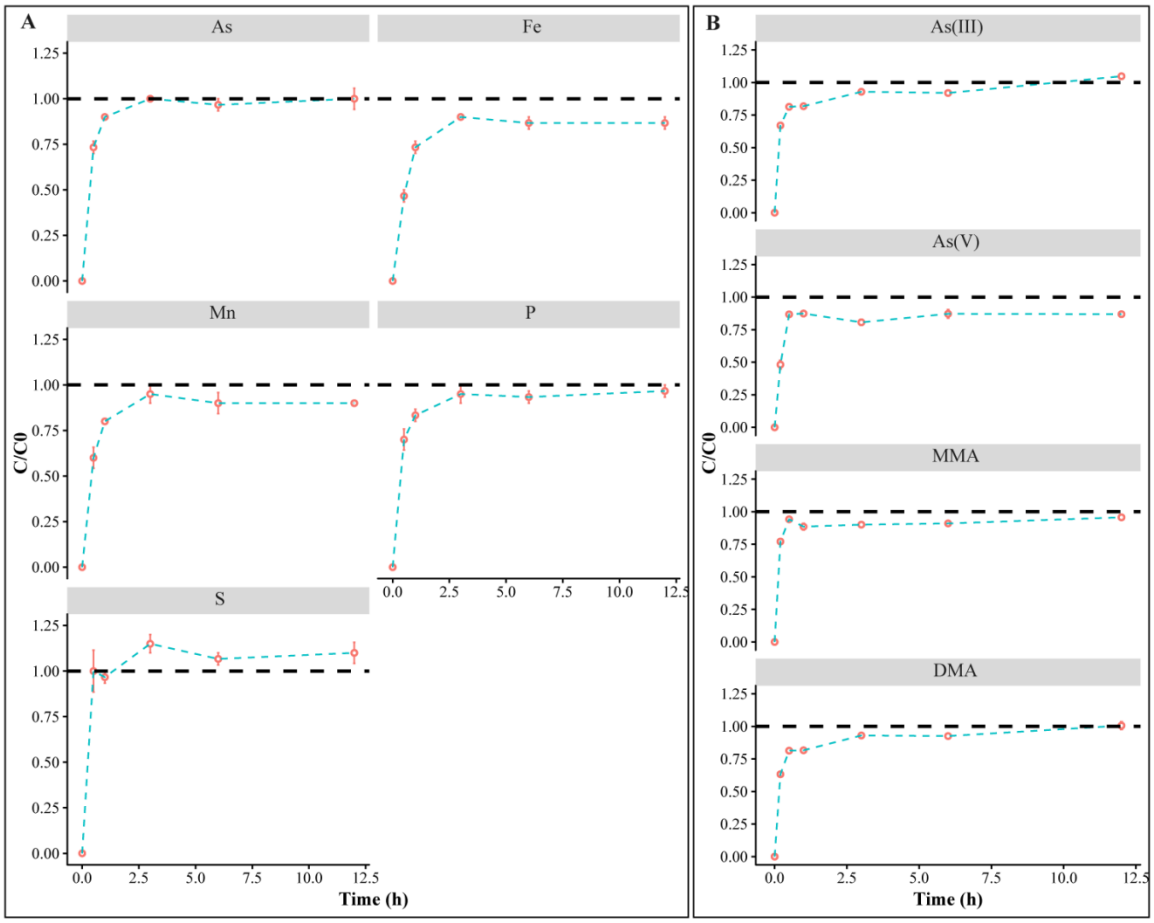

787

788 **Figure S5** The dynamic response of total elements (A) and redox species (B) in IPI
789 samplers (normalized element concentration in solutions). A) total elements include
790 arsenic (As), iron (Fe), manganese (Mn), phosphorus (P) and sulfur (S) measured by
791 ICP-MS; B) four As species, including arsenite [As(III)], arsenate [As(V)],
792 monomethylarsonic (MMA) and dimethylarsinic (DMA), were tested by IC-ICP-MS.
793 The error bar is the standard deviation ($n = 3$).

794

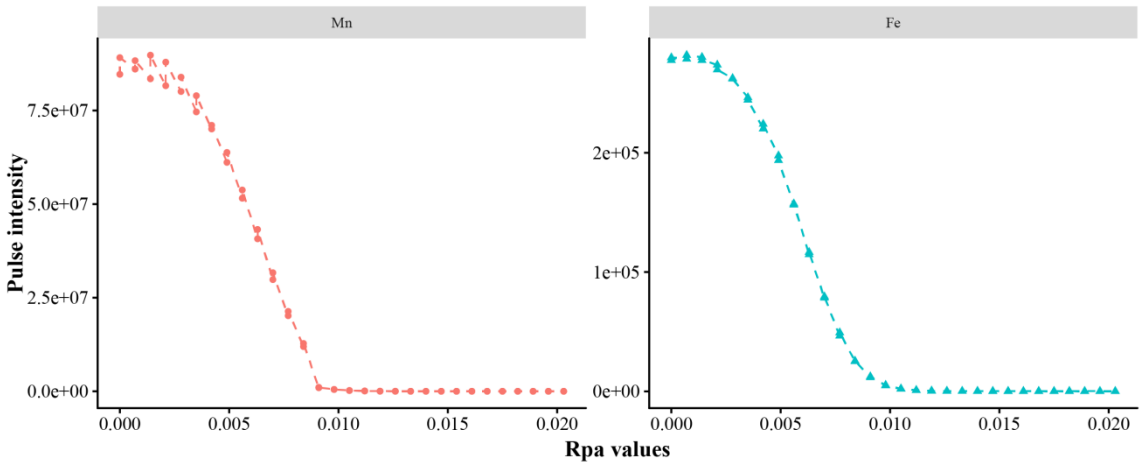

795

796 **Figure S6** Response of Fe and Mn to different Rpa values.

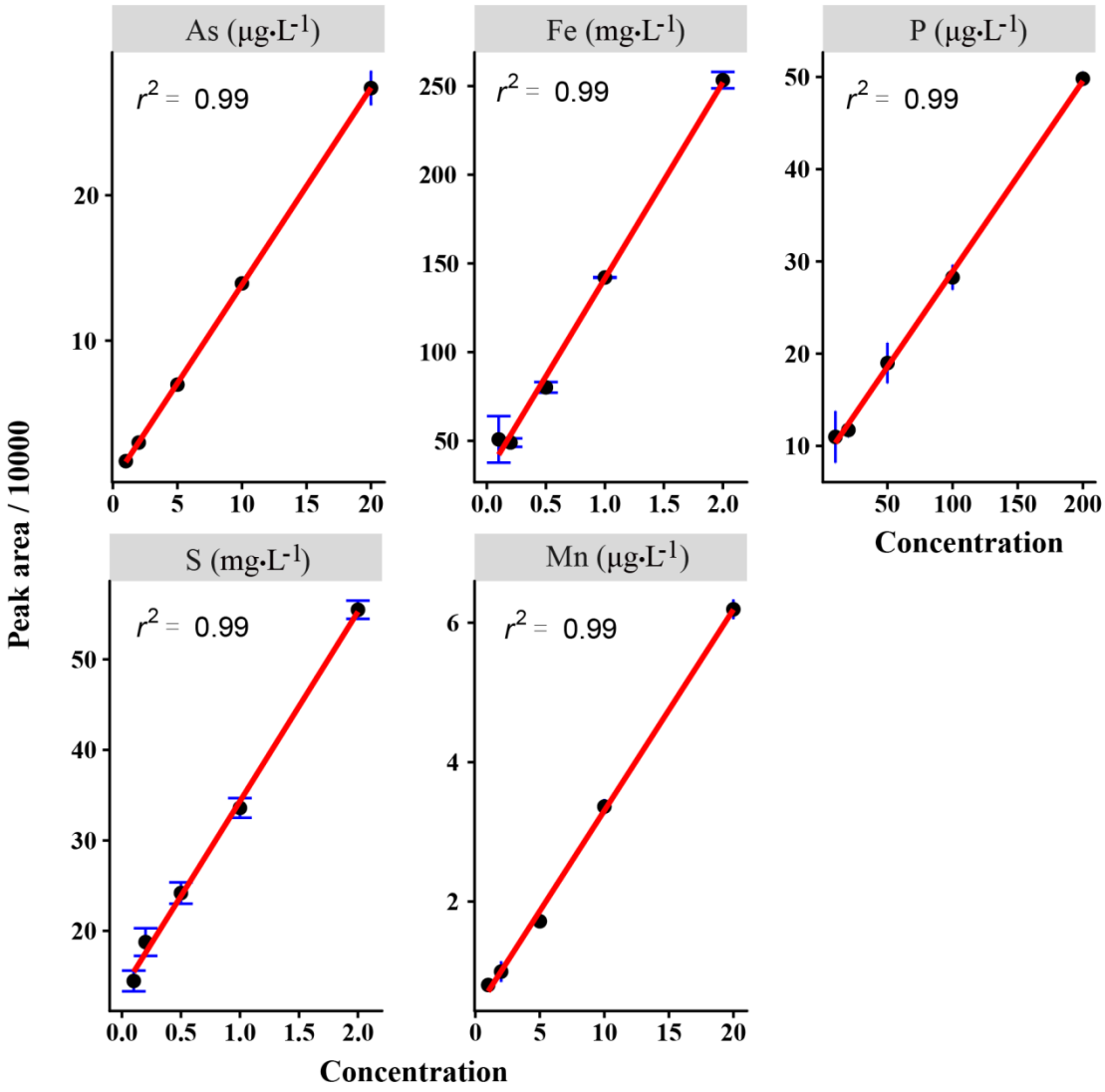

797

798 **Figure S7** The calibration curve of As, Fe, Mn, P, and S (n = 3). The standards,

799 containing 1.0/10/100, 2.0/20/200, 5.0/50/500, 10/100/1000, 20/200/2000 μg·L^{-1}

800 As&Mn/P/Fe&S, were prepared in 2% HNO_3. The error bar is the standard deviation.

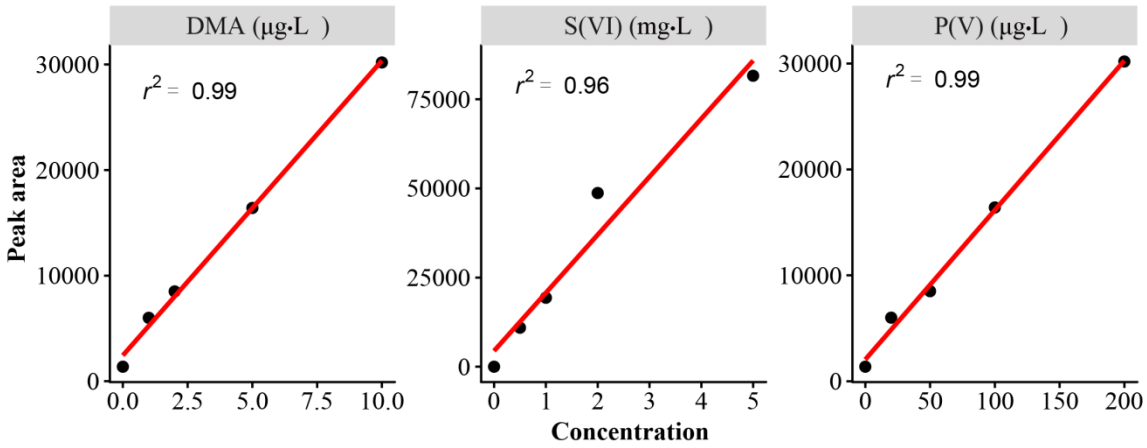

801

802 **Figure S8** The calibration curve of dimethylarsinic (DMA), sulfate (S(VI)) and
803 phosphate (P(V)). The standards, containing 0/0/0, 1.0/20/500, 2.0/50/1000,
804 5.0/100/2000, 10/200/5000 μg·L^{-1} DMA/P(V)/S(VI), were prepared under neutral
805 conditions.

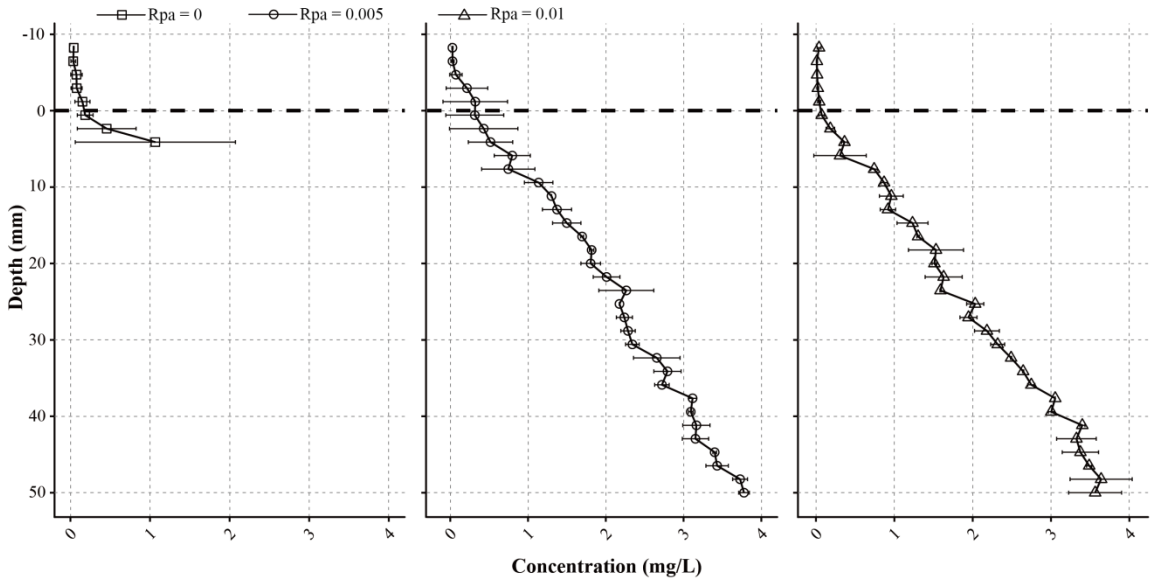

Figure S9 Manganese (Mn) profile measured by ICP-MS with different Rpa values in Shaoguan (SG) paddy. Rpa values were set at 0, 0.005, and 0.01 respectively. The error bar is the standard deviation ($n = 2$).